ACS APPLIED MATERIALS & INTERFACES

Research Article

www.acsami.org

Self-Assembled Poly(ethylene glycol)-*co*-Acrylic Acid Microgels to Inhibit Bacterial Colonization of Synthetic Surfaces

Qichen Wang,[†] Emel Uzunoglu,[†,‡] Yong Wu,[†] and Matthew Libera*[,†]

[†]Department of Chemical Engineering and Materials Science, Stevens Institute of Technology, Hoboken, New Jersey 07030, United States

[‡]Department of Medical Microbiology, Ankara University, Ankara, Turkey

Supporting Information

ABSTRACT: We explored the use of self-assembled microgels to inhibit the bacterial colonization of synthetic surfaces both by modulating surface cell adhesiveness at length scales comparable to bacterial dimensions (~1 μm) and by locally storing/releasing an antimicrobial. Poly(ethylene glycol) [PEG] and poly(ethylene glycol)-*co*-acrylic acid [PEG-AA] microgels were synthesized by suspension photopolymerization. Consistent with macroscopic gels, a pH dependence of both zeta potential and hydrodynamic diameter was observed in AA-containing microgels but not in pure PEG microgels. The microgels were electrostatically deposited onto poly(L-lysine) (PLL) primed silicon to form submonolayer surface coatings. The microgel surface density could be controlled via the deposition time and the microgel concentration in the parent suspension. In addition to their intrinsic antifouling properties, after deposition, the microgels could be loaded with a cationic antimicrobial peptide (L5) because of favorable electrostatic interactions. Loading was significantly higher in PEG-AA microgels than in pure PEG microgels. The modification of PLL-primed Si by unloaded PEG-AA microgels reduced the short-term (6 h) *S. epidermidis* surface colonization by a factor of 2, and the degree of inhibition increased when the average spacing between microgels was reduced. Postdeposition L5 peptide loading into microgels further reduced bacterial colonization to the extent that, after 10 h of *S. epidermidis* culture in tryptic soy broth, the colonization of L5-loaded PEG-AA microgel-modified Si was comparable to the very small level of colonization observed on macroscopic PEG gel controls. The fact that these microgels can be deposited by a nonline-of-sight self-assembly process and hinder bacterial colonization opens the possibility of modifying the surfaces of topographically complex biomedical devices and reduces the rate of biomaterial-associated infection.

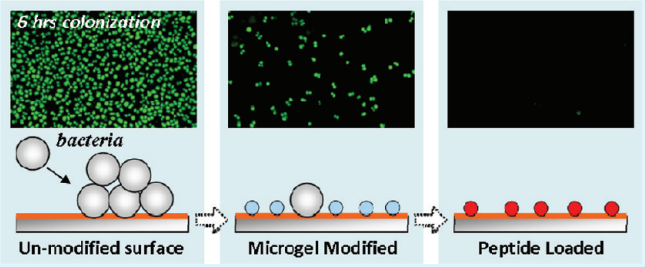

KEYWORDS: *microgels, PEG, self-assembly, patterning, antifouling, bacteria, biofilms, infection*

1. INTRODUCTION

Biomaterial-associated infection occurs when bacteria colonize the surface of a tissue-contacting biomedical device and chronically infect the surrounding tissue. A colonized device typically must be removed and replaced, and the required revision surgery can have a very significant impact on both the patient and the health-care system. A number of strategies are thus being explored to inhibit bacterial colonization of synthetic surfaces. Among these are: antibiotic tethering to or controlled antibiotic release from surfaces and coatings;[1−5] the incorporation of Ag or Cu to locally promote metal-ion release;[6−13] surface presentation of antimicrobial peptides and quaternary ammonium compounds rich in positive charge;[14−20] and the creation of antifouling coatings that resist bacterial adhesion.[21−30] In this latter category, hydrogels and gel-like surfaces have been and continue to be widely studied for use in biomaterial applications because of their ability to control surface interactions with various types of cells.

Among the various materials used for antifouling applications, poly(ethylene glycol) (PEG) is particularly well-known for its resistance to nonspecific protein adsorption and cell adhesion.[31−38] PEG-based materials also resist the adhesion of many bacteria.[23,29,30,39−41] PEG-based materials have been used extensively in the form of continuous films or monolayers to modify surfaces but less so in the form of discontinuous coatings. We have recently shown that discontinuous PEG coatings are nevertheless able to resist the adhesion of bacteria when the length scale of the discontinuities is comparable to that of the bacteria.[42] Specifically, we used a variation of electron-beam lithography to precisely pattern submicrometer-sized microgels of pure PEG on glass substrates at highly controlled intergel spacings. We found that the adhesion rate of staphylococcal bacteria, which are spherically shaped and approximately 1 μm in diameter, decreased substantially relative to the unpatterned glass control when the intergel spacing was 1.5 μm and below. Significantly, however, we found that osteoblast-like cells are still able to adhere to these patterned surfaces despite the nonadhesive microgels.

Received: February 4, 2012
Accepted: April 22, 2012
Published: April 22, 2012

Here, we explore an alternate method to create surfaces with modulated adhesiveness to cells, bacteria, and proteins. Rather than use electron-beam patterned microgels, we modulate surface adhesiveness using suspension-polymerized PEG-based microgels deposited by electrostatic self-assembly. In contrast to the electron-beam approach, this self-assembly method gives up the ability to precisely control both the microgel size and spacing on a surface. However, since it is a nonline-of-sight deposition method, self-assembly provides the ability to coat topographically complex surfaces such as the roughened implants often used in implanted hip and knee prostheses. Furthermore, self-assembly is a parallel deposition process that can simultaneously modify large areas of surface, whereas electron-beam patterning is a serial process better suited for a small area. Suspension polymerization also affords greater flexibility in defining the microgel composition, and here, we study not only pure PEG microgels but also microgels made by copolymerizing PEG and acrylic acid (AA). At physiological pH, the deprotonated AA acid groups facilitate electrostatic deposition, and they enhance the microgel adsorption to poly(L-lysine) primed silicon substrates. This electrostatic charge also promotes postdeposition microgel loading by a cationic antimicrobial peptide. We find that the loading is significantly higher in the PEG-AA microgels than in the pure PEG microgels. Surfaces modified by self-assembled microgels all exhibit a reduced susceptibility to bacterial colonization, the extent of which can be tuned by controlling the extent of surface modification and antimicrobial loading inside the microgels.

2. EXPERIMENTAL METHODS

2.1. Microgel and Bulk Gel Synthesis. Microgels were synthesized using surfactant-free suspension polymerization. Pure PEG microgels and PEG containing 10 vol % AA (denoted here as PEG-AA) were studied. Prior to use, in order to remove inhibitor, poly(ethylene glycol) diacrylate (PEGDA, average M_n 575, Sigma Aldrich) was washed 5 times in hexane, and AA (Acros Organics) was distilled at 50 °C under reduced pressure. PEGDA (200 μL), AA (0 or 20 μL), and photoinitiator (10 μL, Darocur 1173, Ciba) were dissolved in dichloromethane (1 mL, DCM, Acros Organics) to obtain a precursor solution. Deionized water (DI water, 10 mL, Millipore, 18.2 MΩ-cm) was dripped into the precursor solution while magnetically stirring (1000 rpm) until an inverse emulsion formed, and the resulting emulsion was further refined by sonication (Cole-Parmer; 100 W) for 20 min. The emulsion was then exposed to light from a low-pressure ozone-producing ultraviolet (UV) grid lamp for 15 min to drive the free-radical polymerization under continuous sonication. The resulting microgels were washed in ethanol 3 times and DI water 3 times. The final suspension was filtered with a 1.0 μm pore size glass fiber membrane (Corning) to remove larger microgels.

Bulk gel was synthesized from the same precursor solution used in the microgel synthesis. Instead of forming an emulsion, however, the precursor solution was covered with a layer of water to minimize DCM evaporation during polymerization, and the solution was exposed to UV light for 15 min. The resulting gels were dried overnight (50 °C) to remove DCM. These gels typically had a dry mass of ∼0.2 g with dimensions on the order of millimeters, and we refer to them here as bulk gels to differentiate them from the microgels with microscopic dimensions.

2.2. FTIR Analysis. Fourier-transform infrared (FTIR) spectroscopy was used to confirm the PEG-AA microgel composition. Standard compositions were prepared by mixing poly(acrylic acid) homopolymer (PAA, M_w =1800, Sigma Aldrich) and PEG bulk gel (synthesized from PEGDA 575) with mole ratios of AA monomer to ethylene glycol (EG) monomer of 0, 0.02, 0.05, 0.1, and 0.2. Note that each PEGDA 575 molecule on average contains 10 ethylene glycol monomer units. These samples, as well as samples of pure PAA homopolymer, pure hydroxy-terminated PEG homopolymer (M_w = 6800, Scientific Polymer Products), and dried PEG-AA microgels were blended with KBr. The infrared absorbance was measured (Perkin-Elmer Paragon 1000PC) at wavenumbers between 900 and 4000 cm^{-1}.

2.3. Gel Swelling and Zeta Potential Measurement. Microgel and bulk gel swelling in 0.01 mol/L phosphate buffer within the pH range of 2 to 9 was studied. Microgels were suspended in buffer at a specific pH for 2 h, and then their hydrodynamic diameter and zeta potential were measured using a Malvern Zetasizer. Bulk gel swelling behavior was characterized by the volume swell ratio, q. As-synthesized gel was dried overnight at 50 °C. Each gel was then rehydrated by soaking overnight in buffer at a specific pH, and the hydrated weight, w_h, was measured. After again drying, the dry weight, w_d, was measured. The swell ratio was calculated from:

$$q = \frac{(w_h - w_d)/\rho_{water} + w_d/\rho_{PEGDA}}{w_d/\rho_{PEGDA}} \quad (1)$$

where ρ_{water} and ρ_{PEGDA} are the density of water and PEGDA (1.12 g/cm^3), respectively. Three gels were studied at each pH value examined.

2.4. Gel Mesh Size. The gel mesh size, ξ, is the average distance between adjacent cross-links in the gel network. We estimated it using the classical swelling theory originally developed by Flory and Rehner:[43−45]

$$\xi = (\overline{r_0^2})^{1/2} v_{2m}^{-1/3} \quad (2)$$

where v_{2m} is the volume fraction of polymer in the swollen gel and is inversely related to the volume swell ratio, q:

$$v_{2m} = \frac{V_p}{V_s} = \frac{volume\ of\ polymer\ in\ dry\ gel}{volume\ of\ hydrated\ gel} = \frac{1}{q} \quad (3)$$

The average end-to-end distance, $(\overline{r_0^2})^{1/2}$, can be estimated from:

$$(\overline{r_0^2})^{1/2} = C_n^{1/2} n^{1/2} l \quad (4)$$

Here, l is the average bond length (0.147 nm); C_n is the characteristic ratio, which we have taken for PEG to be 4.0;[46,47] and n is average number of bonds between cross-links, which for a pure PEG gel is given as $n = 3 \times (M_c/44\ Da)$. M_c is the average molecular weight between cross-links, and 44 Da is the molecular weight of the PEG monomer. M_c can be determined from:[43,48−50]

$$-[\ln(1 - v_{2m}) + v_{2m} + \chi(v_{2m})^2] = \left[\frac{v_l}{\overline{v} M_c}\right]\left[v_{2m}^{1/3} - \frac{v_{2m}}{2}\right] \quad (5)$$

where $\overline{v}$ is specific volume of PEG (0.893 cm^3/g), v_l is molar volume of water (18 cm^3/mol), and χ is the Flory−Huggins interaction parameter, which we assumed to be 0.426.[47,50,51]

2.5. Microgel Deposition. Microgels of PEG and PEG-AA were deposited onto poly (L-lysine) [PLL] primed polished Si single-crystal wafer substrates (5 × 7 mm, Ted Pella). The wafers were rinsed with DI water and 70% EtOH, soaked in 98% H_2SO_4 overnight, and rinsed again with DI water. They were then exposed to 1 mol/L NaOH for 15 min to form a negatively charged surface and immersed in aqueous PLL solution (0.2 mg/mL, PLL M_w >30k, Sigma Aldrich, pH 9) for 2 h. PLL has a pK_a of 10.53, and the surface silanol groups on which the PLL was deposited have a pK_a of 9.1−9.4. At pH 9, ∼97% of the PLL amine groups were protonated and thus positively charged, while ∼50% of the silanol groups were deprotonated and, hence, negatively charged.[52] The PLL-primed Si wafers were rinsed with phosphate buffer (pH 7.4, 0.01 mol/L) and DI water and dried with flowing N_2 gas. PLL deposition was confirmed by ellipsometry.

To deposit microgels, the PLL-primed substrates were immersed in a microgel suspension at a concentration of either 1.4×10^{10} particles/mL or 1.4×10^{11} particles/mL at pH 7.4 for time periods ranging from 0.5 to 10 h. After deposition, the microgel-modified wafers were rinsed with pH 7.4 phosphate buffer and DI water, dried in air, and imaged by scanning electron microscopy (SEM; Zeiss Auriga). The number of

particles per unit area on each surface was determined by analyzing SEM images collected at a magnification of 10 kx from nine different specimen locations. The diameters of approximately 500 microgels, either PEG or PEG-AA, were measured using the ImageJ software platform.[53] A Rosin-Rammler model[54] was used to model the size distribution of the deposited microgels:

$$P = 100 \times \left\{1 - \exp\left[-\left(\frac{d}{D_m}\right)^n\right]\right\} \quad (6)$$

where d is the dry microgel particle diameter; D_m is mean microgel diameter; n is measure of the spread of particle diameter; and P is the cumulative percentage of microgels smaller than d.

2.6. Antimicrobial Peptide Loading. Loading of an antimicrobial agent to surface-bound microgels used an 18-residue cationic oligopeptide designated as L5 with the sequence PAWRKAFRWAWRMLKKAA.[55] It contains 6 cationic amino acids (R and K) and no anionic amino acids, and it has a molecular weight of 2274 Da. L5 was synthesized by GenScript (Piscataway, NJ) with and without a fluoroscein isothiocyanate (FITC) label at its N-terminus (designated as FITC-L5). L5 or FITC-L5 aqueous solution (20 μL, 1 mg/mL, pH 6.5) was dropped onto a microgel-modified surface, left to stand for 2 h, and then washed with DI water and allowed to dry in air. The FITC-L5 infiltration was demonstrated using confocal laser scanning microscopy (Nikon E1000 C1). The extent of peptide loading was quantified using a Bradford protein assay and using atomic force microscopy (AFM, Pacific Nanotechnology Nano-R) under a controlled humidity of 25%.

2.7. Peptide Antimicrobial Susceptibility Test. The MIC (minimum inhibitory concentration) and MBC (minimum bactericidal concentration) were determined by the broth microdilution method following a modified M7-A8 protocol of the CLSI (Clinical and Laboratory Standards Institute).[56] These tests used a clinical strain (NJ 9709) of *S. epidermidis* collected from an infected catheter.[57] Cation-adjusted Muller-Hinton broth (CAMHB; 150 μL) with L5 was added to separate wells on 96-well polypropylene microtiter plates. Each well was then inoculated with 50 μL of bacteria in CAMHB. The final concentrations of L5 were 512, 256, 128, 64, 32, 16, 8, 4, 2, 1, 0.5, and 0.25 μg/mL, and the final bacterial concentration was 2.5×10^7 CFU/mL. The plates were incubated at 37 °C for 24 h, and then the optical density (OD) of each well was measured at 600 nm. The MIC was defined to be the lowest concentration at which there was negligible turbidity. Solutions from concentrations at or above the MIC were used to inoculate sheep blood agar plates. These agar plates were incubated for 24 h at 37 °C. The MBC was defined as the concentration at or above which there was no visible bacteria growth. Vancomycin (Sigma Aldrich) was used as a control.

2.8. Assessment of Bacteria–Surface Interactions. The ability of bacteria to colonize both modified and control surfaces was assessed by evaluating the extent of bacterial colonized area fraction on different surfaces using the clinical strain (NJ 9709) of *S. epidermidis*. This strain was cultivated on sheep blood agar plates overnight at 37 °C. A few colonies were then suspended in 20 mL of modified tryptic soy broth (30 g/L tryptic soy broth with 6 g/L yeast extract and 8 g/L glucose) and cultured in 100 × 15 mm Petri dishes for 18 h at 37 °C. Colonies on the bottom of the Petri dish were washed with PBS three times, scraped, suspended in PBS, vortexed, and then passed through a 5 μm filter (Millipore). The concentration of bacteria was determined using a Petroff-Hauser counting chamber.

We studied the bacterial response to seven different surfaces: (i) cleaned but unmodified Si wafer (Si); (ii) PLL-primed Si (PLL); (iii) pure PEG bulk gel cut into 1 mm × 5 mm × 7 mm films (PEG gel); (iv) low-density (~0.4 particles/μm^2) PEG-AA microgel-modified Si (low PEG-AA); (v) peptide-loaded low-density PEG-AA (low PEG-AA w/L5); (vi) high-density (~1.2–1.4 particles/μm^2) PEG-AA microgel-modified Si (high PEG-AA); and (vii) peptide-loaded high-density PEG-AA (high PEG-AA w/L5). Surfaces (v) and (vii) used non-FITC-labeled L5 peptide. Each substrate was immersed in an inoculum of *S. epidermidis* suspended in PBS (~2.5×10^7 CFU/mL) to allow bacterial adhesion. After 30 min, the inoculum was removed, and the substrate was gently rinsed with PBS to remove weakly adhered bacteria. The inoculated surfaces were then incubated in fresh modified TSB at 37 °C for 2, 6, and 10 h. The medium was changed every 2 h. At each of three time points, medium was removed, and a subset of substrates was gently rinsed with PBS, fixed in 4% paraformaldehyde for 20 min, and stained with SYTO 9 for confocal imaging. SYTO 9 provides high contrast with which to threshold such images between colonized and exposed surface. Nine different positions were imaged on each substrate surface, and for each time point, three different copies of each of the seven surfaces were studied. The area fraction colonized by bacteria was calculated using the ImageJ software platform.[53]

3. RESULTS AND DISCUSSION

3.1. FTIR Analysis. FTIR spectroscopy confirmed the composition of the PEG-AA microgel sample. Hydroxy-terminated PEG homopolymer (PEG–OH) shows absorbance (Figure 1A) in the region of 990–1220 cm^{-1} centered at 1104 cm^{-1}, which indicates the ether linkage (C–O–C), but there is no obvious absorbance in the region of 1500–1900 cm^{-1} centered at 1730 cm^{-1} which indicates the carbonyl (C=O). The PEG bulk gel shows absorbance in both regions, but the absorbance in the C=O region, due to the ester-linked acrylate end groups, is less than that of the pure PAA homopolymer. We thus used the intensity ratio of the C=O and C–O–C peaks as a means to quantify composition. A standard curve was created by plotting the ratio of absorbance from 1500 to 1900 cm^{-1} to that from 990 to 1220 cm^{-1} from specimens with

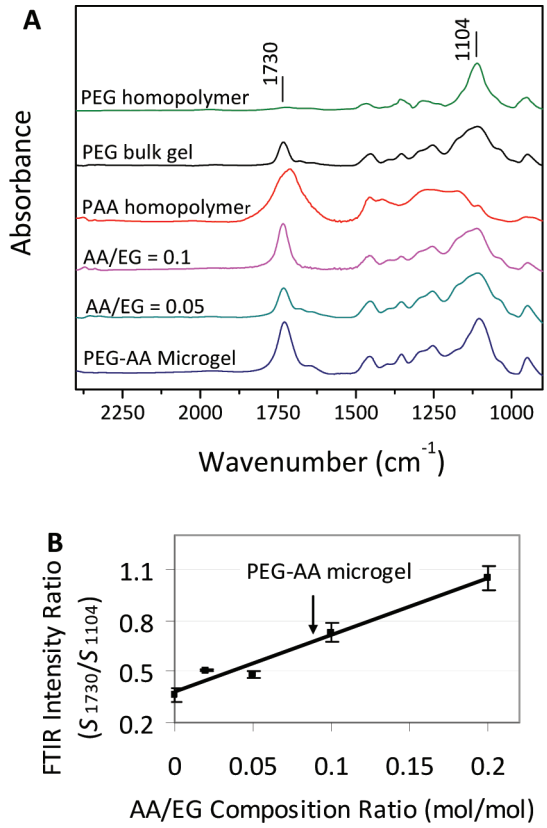

Figure 1. (A) FTIR spectra of various PEG, PAA, and gel compositions. (B) Calibration curve relating FTIR peak intensity ratios (S_{1730}/S_{1104}) to gel composition. Spectra from known absorbance peak area ratios of AA and EG regions were used to generate a calibration curve (B), from which the PEG-AA microgel composition can be calculated.

known ratios of PEG gel and PAA homopolymer (Figure 1B). From this, the mole ratio of AA monomer to EG monomer in the PEG-AA microgel sample was determined to be 0.09, which corresponds to 12 vol % and is close to the 10 vol % value expected from the microgel synthesis protocol.

3.2. pH-Dependent Gel/Microgel Properties. We studied bulk gels to determine the effect of AA on the swelling behavior in different pH conditions (Figure 2). Additional

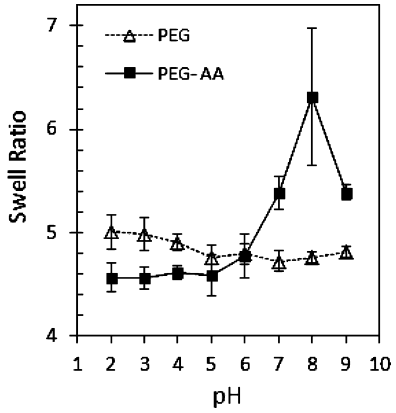

Figure 2. pH-dependent swell ratios of PEG and PEG-AA bulk gels. Each data point represents the average of measurements on three nominally identical gels. Error bars correspond to the standard deviation about the average.

experimental data describing different compositions and solvents used during synthesis are provided as Supporting Information (Figure S1). Due to the absence of charge, the swell ratio of the pure PEG gel shows no significant dependence on pH. Relative to pure PEG gels, adding 10 vol % AA slightly decreases the swell ratio at lower pH (Figure 2). In addition to the covalent cross-links introduced during the acrylate polymerization, at lower pH values, additional cross-links are formed by hydrogen bonding between AA protonated carboxyls and PEG ether oxygens.[58] At higher pH, however, the swell ratio increases. The transition occurs at pH values between 6 and 7, which is consistent with measurements by Choi and Rubner[59] on the pH-dependent degree of ionization of PAA. The carboxyl ionization not only disrupts the AA-PEG hydrogen bonding but also increases the electrostatic repulsion between the deprotonated AA groups.

Microgels exhibit similar pH-dependent swelling behavior (Figure 3A) as well as a corresponding pH-sensitive zeta potential (Figure 3B). The PEG microgels show only slight changes in both their hydrodynamic diameter and zeta potential between pH 2–9. However, PEG-AA microgels show an increasing hydrodynamic diameter and a decreasing zeta potential with increasing pH confirming that the copolymerized AA in the microgels introduces anionic character at higher pH.

3.3. Microgel Deposition. The SEM images of Figure 4 describe PLL-primed surfaces that were modified by PEG (Figure 4A) and PEG-AA (Figure 4B) microgels and then dried. The size distributions of the dry microgel diameters (Figure 4C) correspond to a Rosin-Rammler model. Fitting these data to eq 6 shows that the PEG and PEG-AA microgels have mean diameters of 196 and 309 nm, respectively (Table 1). Note that these dry-size data, together with the average hydrodynamic diameters (Figure 3A), are roughly consistent

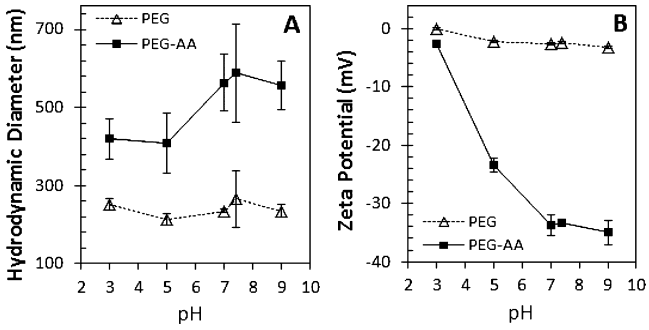

Figure 3. pH-dependent hydrated average diameter (A) and zeta potential (B) of microgels. Each data point represents the average of at least three different measurements, and error bars correspond to the standard deviation about the average. Note that the reproducibility of the zeta-potential measurement of pure PEG microgels (B) is smaller than the symbol size depicting the average value.

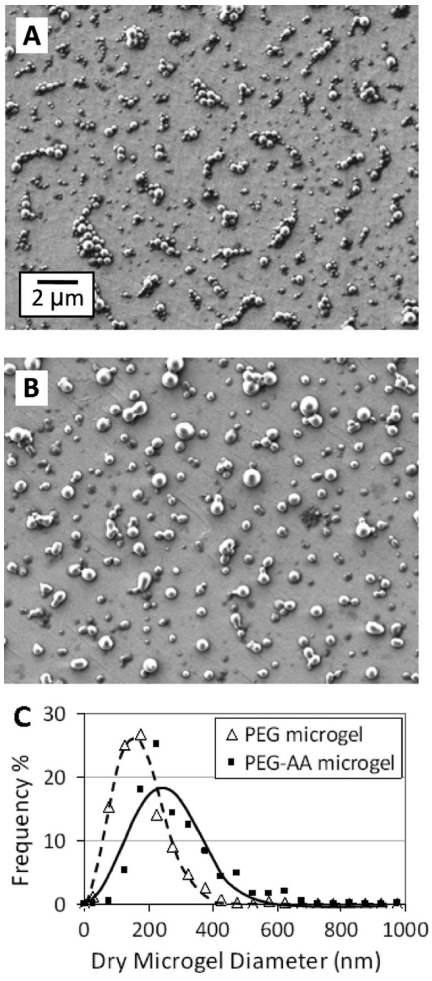

Figure 4. SEM images of (A) PEG and (B) PEG-AA microgels deposited for 3 h on PLL-primed Si from a solution containing in 1.4 × 10^{11} microgels/mL. (C) The size distribution of dry microgels.

Table 1. Size Distribution Properties of Dry Microgels

microgel composition	mean diameter (nm)	(variance)$^{1/2}$ (nm)
PEG	196	77
PEG-AA	309	110

dx.doi.org/10.1021/am300197m | ACS Appl. Mater. Interfaces 2012, 4, 2498–2506

with the volume swelling properties of the bulk gels at pH 7.4 (Figure 2): $(280/196)^3 = 2.9$ and $(580/309)^3 = 6.6$ for the pure PEG and PEG-AA microgels, respectively.

The microgel adsorption kinetics are described by Figure 5, which presents the microgel particle packing density (Figure 5A) and the percent of surface area covered by hydrated microgels (Figure 5B) as a function of time. The hydrated surface covered data are derived from measurements of the number of dry microgels per unit area (Figure 5A) multiplied by the average hydrated microgel projected area. Figure 5 shows that the surface packing density of both the PEG and PEG-AA microgels can be controlled by means of the deposition time and the microgel concentration in suspension. In both systems, increasing the concentration of microgels in the parent colloidal suspension for a given deposition time increases the microgel density on the substrate surface. The initial deposition rate is relatively high, and then this rate asymptotically approaches zero as the surface coverage approaches a sub-monolayer limit. This kinetic behavior as well as the fact that the surfaces do not become fully covered by microgels is consistent with the random sequential adsorption (RSA) theory[60] and is a consequence of repulsion between microgels.[61] During deposition, the microgels are sequentially adsorbed onto the substrate surface and become immobilized there. When the spacing between adsorbed microgels approaches the average microgel diameter, the ability of additional microgels to adsorb decreases because the repulsive microgel−microgel interactions begin to compete with the adhesive microgel−surface interactions. To increase the surface coverage further would require, for example, changes in solution pH or salt concentration,[61] incorporation of oppositely charged polymer layers to offset interparticle repulsion using a layer-by-layer approach,[62] or an additional driving force such as centrifugation.[63] We note that there is a greater number of agglomerated microgels in the PEG sample (Figure 4A) than in the PEG-AA sample (Figure 4B). We speculate that such agglomerations are due to surface reorganization due to capillary effects during drying from water and is more pronounced with the PEG microgels because of their weaker interaction with the underlying substrate.

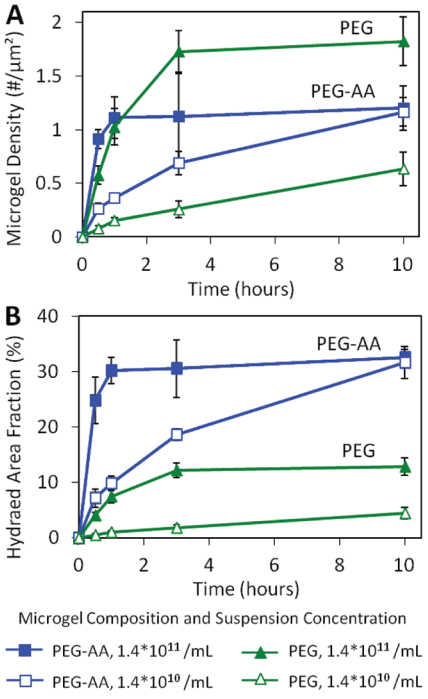

Figure 5. The microgel surface coverage in terms of the (A) number density and (B) area fraction covered by hydrated microgels as a function of deposition time and microgel concentration in solution. Each data point represents the average of measurements from nine different images, and the error bars correspond to the standard deviation about the average.

3.4. Antimicrobial Peptide Loading. Figure 6 presents confocal images assessing the loading of the L5 oligopeptide into both the PEG and PEG-AA microgels deposited on PLL-primed modified silicon substrates. After microgel deposition, these surfaces were exposed to solutions of either FITC (control; Figure 6A,B) or FITC-labeled L5 peptide (C−F). The microgel positions can be imaged using an excitation wavelength of 633 nm, which is insufficiently energetic to excite the FITC, and detecting with high gain using a threshold filter transmitting 650 nm and above. Because the microgels absorb a small fraction of the incident and substrate-scattered light, they appear with dark contrast on an otherwise bright background (Figure 6A,C,E). FITC and FITC-labeled L5 were detected using an excitation wavelength of 488 nm. The absence of green fluorescence in Figure 6B indicates that FITC by itself does not interact strongly with the PEG-AA microgels. However, the green fluorescence in Figure 6D,F is correlated with the microgel positions in Figure 6C,E, respectively, and confirms that FITC-L5 can be loaded by self-assembly into the microgels.

The peptide can infiltrate the microgel particles if the gel-mesh size is at least as large as the peptide. The mesh size can be estimated from the swell ratio. For a swell ratio of 3, eqs 2 through 5 indicate that the mesh size of such a gel would be 2.3 nm. The peptide size was estimated by two methods. The Chou-Fasman method to predict the secondary structure[64] suggests that L5 is an α helix with dimensions of approximately 1 nm in diameter by 2.7 nm in length. If instead the L5 peptide adopts a random-coil conformation, its radius of R_{pep} can be estimated by:[65,66]

$$\frac{4}{3}\pi {R_{pep}}^3 = \left(\frac{\overline{\nu_{pep}} M}{N_{AV}}\right) \quad (7)$$

where the specific volume of the aqueous protein, $\overline{\nu_{pep}}$, is 0.73 cm^3/g, M is its molecular weight (2274 Da), and N_{AV} is Avogadro's number. Equation 7 predicts that the diameter of the spherical peptide would be $2R_{pep}$ = 1.8 nm. Both methods indicate that the L5 is physically smaller than the mesh size of both the PEG and PEG-AA microgels. Hence, there is no physical barrier to L5 loading.

The fluorescence intensity of the various microgels in Figure 6B,D,F are plotted in Figure 6G as a function of the microgel volume. The intensity values correspond to the sum of the counts per pixel for all of the pixels associated with a particular microgel divided by 4000, the camera pixel saturation value. The lines represent linear least-squares fits to each data set, and the fact that there is a linear relationship between the emitted intensity and the microgel volume indicates that the microgel diameter is, on average, less than the z resolution of the confocal collection system. The difference in slope indicates that approximately four times more L5 is loaded into the AA-containing microgels than in the pure PEG microgels.

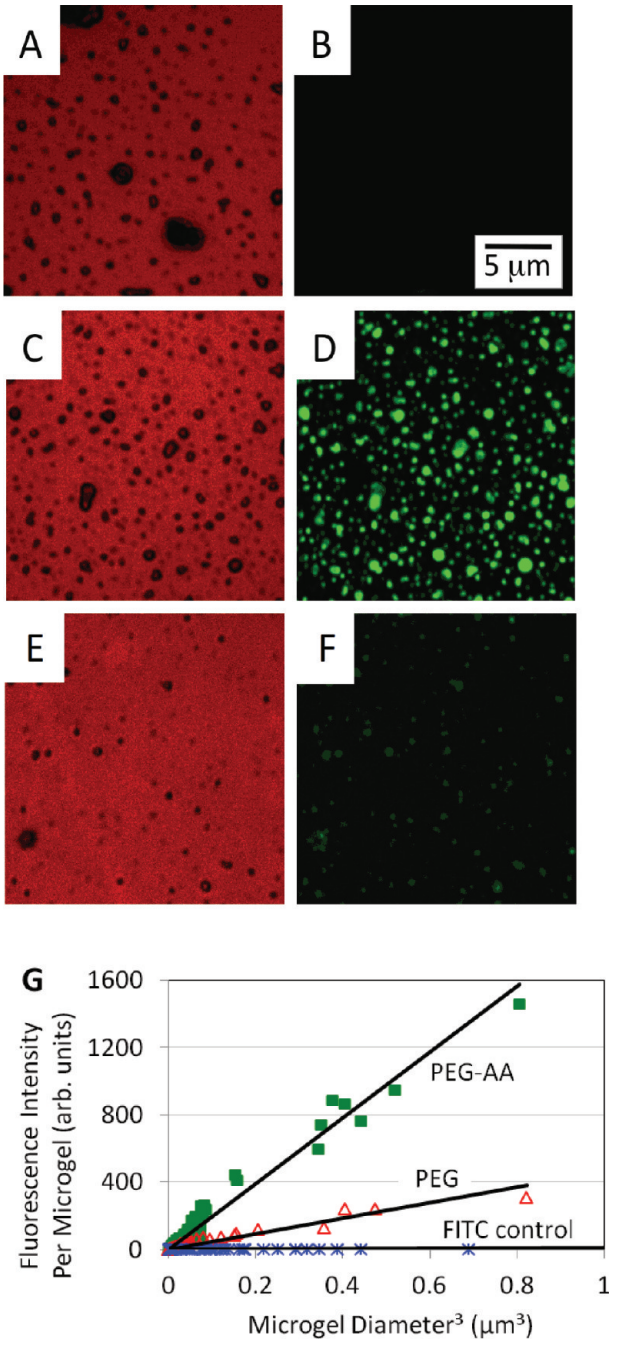

Figure 6. Confocal images of gel-modified surfaces using 633/650LP nm excitation/detection to show microgel positions (A, C, E) and 488/(515/30) nm excitation/detection to indicate FITC. FITC is not observed when surfaces are exposed to FITC control (B) but is correlated with microgel positions when surfaces are exposed to FITC-labeled L5 (D, F). PEG-AA microgels (D) show higher fluorescence intensity than PEG microgels (F). (G) The fluorescence intensity analysis confirms that the PEG-AA microgels absorb more L5 than PEG microgels.

An estimate of the peptide diffusivity into the microgels indicates that the loading difference is not a kinetic effect. Following Lustig and Peppas,[67] the diffusivity of a solute, D_s, with a characteristic size of 1.8 nm in a hydrated gel with a swell ratio of 3 and a mesh size of 2.3 nm is about an order of magnitude less than that of the peptide in pure water ($\sim 10^{-10}$ m^2/s). Note that these gel properties are the most tortuous of those observed in our experiments, so using a $D_s = 10^{-11}$ m^2/s represents a lower bound to the peptide diffusivity in the microgel. The solution to the diffusion equation for radial diffusion into a sphere is known[68] and predicts that the average solute composition at the center of a 1 μm diameter gel, an upper bound to the microgel size used here, reaches 0.99 that of the surrounding solution in approximately 100 ms, a time scale several orders of magnitude below that used here for peptide loading. We can thus attribute the different loading of the PEG and PEG-AA microgels to thermodynamic effects rather than to mesh-size-dependent kinetic effects. The fact that the pure PEG microgels bind L5 can be attributed to the interaction between the PEG ether oxygens and the peptide amine groups. The AA-containing microgels, however, have the additional stronger ionic interactions between the deprotonated carboxyls on the copolymerized AA groups and the L5 amine groups.

Since the loading of L5 into the AA-containing microgels is so much greater than in the pure PEG microgels, we concentrated our experiments on bacteria-surface interactions using only the PEG-AA microgels. Specifically, we studied PLL-primed silicon modified by PEG-AA microgels with either a low or a high surface coverage of 0.4 and 1.2 particles/μm^2, respectively. We quantified the extent of L5 loading in the PEG-AA microgels using both the Bradford protein assay and AFM imaging. The protein assay indicates that the amount of L5 loaded is 3.4 ± 1.1 and 5.7 ± 2.5 $\mu g/cm^2$, respectively, for the low-density and high-density PEG-AA microgel-modified surfaces. These values are corroborated by AFM images taken from dry microgels both before and after loading (Figure 7).

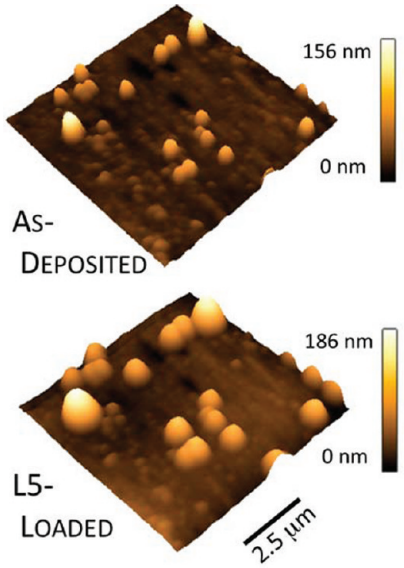

Figure 7. AFM images of the same area of dry surface with PEG-AA microgels before (top) and after (bottom) L5 loading.

Analysis of the microgel volume change from these AFM images indicates the average microgel dry volume increased about 2 times due to the L5 loading. Using the number of microgels per unit area (Figure 5A) and assuming each microgel maintains a spherical shape gives a concentration of L5 at the surface of 0.5 and 1.6 $\mu g/cm^2$, respectively. These values are roughly consistent with those measured by the Bradford assay.

dx.doi.org/10.1021/am300197m | ACS Appl. Mater. Interfaces 2012, 4, 2498−2506

3.5. Bacterial Response to Microgel-Modified Surfaces. Figure 8 shows the results of the MIC and MBC tests.

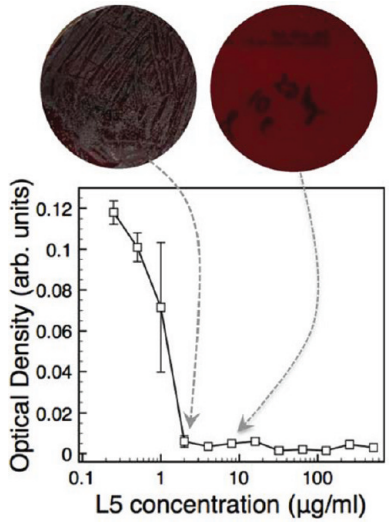

Figure 8. Antimicrobial susceptibility testing (lower graph) shows that the L5 peptide prevents *S. epidermidis* growth at an MIC of 2 μg/mL. Images of sheep blood agar plates (top) indicate an MBC of 8 μg/mL. Each data point represents the average of three from three different culture experiments, and the error bars correspond to the standard deviation about the average.

Wells containing 2−512 μg/mL L5 show decreased optical absorbance relative to wells with a lower L5 concentration, and this finding indicates that 2 μg/mL is the MIC of L5 for NJ 9709 *S. epidermidis*. Culture aliquots plated on sheep blood agar for 24 h indicate that the MBC is 8 μg/mL. Additional data on bacterial susceptibility to both L5 and vancomycin is given as Supporting Information (Table S1).

The *S. epidermidis* response to the seven surfaces is shown in Figure 9. The various surfaces show little difference after 2 h of culture. In particular, the area fraction covered by bacteria on adhesive surfaces, unmodified Si and PLL-primed Si, at this time point is low, since the bacteria had an opportunity to go through only a few doubling cycles. The differences between the various surfaces become clear after 6 h of culture. At one extreme are the unmodified Si and the PLL-primed silicon. Over 40% of each of these surfaces is covered by bacteria. Importantly, both of the unloaded microgel-modified surfaces show significantly less colonization. Furthermore, the colonization resistance of the high-density microgel-modified surface is greater than that of the low-density microgel-modified surface at the 6 h time point. These findings are consistent with the idea that a surface whose cell adhesiveness is laterally modulated at length scales comparable to bacteria is less likely to become colonized than an equivalent unmodified surface.[42] Staphylococci are spherical and typically about 1 μm in diameter. A surface coverage on the order of ~1 microgel /μm^2 should decrease the probability of bacterial adhesion relative to an unmodified surface because, at such a surface coverage, an approaching bacterium would on average interact with at least one repulsive surface feature. Even if cell-adhesive surface is exposed, its ability to resist bacterial adhesion should increase as the average spacing between gel particles decreases. Note, however, that the effect of the modulated surface is lost after 10 h of culture where the bacterial coverage is much the same as on an unmodified surface. This finding indicates that, while a surface with modulated adhesiveness can reduce bacterial adhesion, it does not necessarily inhibit the growth of those bacteria that have adhered, and it speaks to the need for an additional inhibitory mechanism such as antimicrobial release or, in vivo, macrophage activity associated with the inflammatory response.

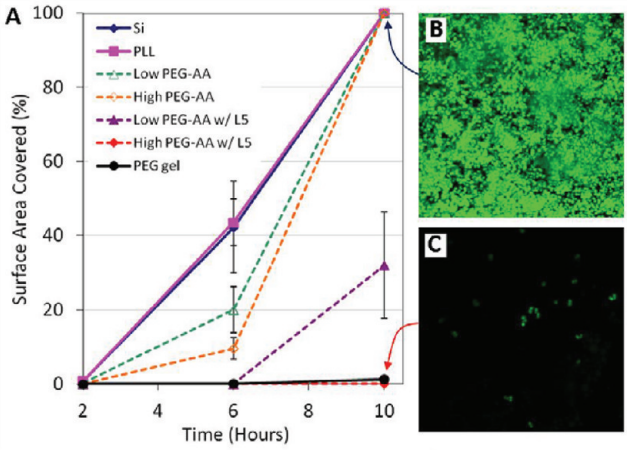

Figure 9. Short-term *S. epidermidis* colonization of various surfaces (A) with confocal images after inoculation and 10 h of culture on silicon (B) and an L5-loaded microgel-modified surface (C). Each data point represents the average of three different culture experiments, and the error bars correspond to the standard deviation about the average.

Loading the surface-bound microgels with the L5 antimicrobial peptide significantly enhances the resistance of the microgel-modified surfaces to staphylococcal colonization. This is most clear in the case of the high-density L5-loaded microgel-modified surface (Figure 9). Colonization of this surface by *S. epidermidis* is as low as that of a continuous surface of PEG gel. As Figure 9C indicates, after 10 h of culture, few bacteria are found on this L5-loaded surface, and these are found only in pairs or singly. Such inhibition can be attributed to the presence of L5. The low-density L5-loaded microgel-modified surface exhibits similar colonization resistance up to the 6 h time point. However, this surface becomes significantly colonized after 10 h, suggesting that the finite L5 supply on this surface becomes depleted over time.

From a phenomenological point of view, we can consider the initial L5 surface concentration to exceed both the MIC and the MBC. The protein assay indicates that the L5 surface concentrations, $C_{L5}^{surface}$, were 3.4 and 5.7 μg/cm^2 for the low-density and high-density microgel-modified surfaces, respectively. In the adhesion step, if some distance of action, h, is assumed from the surface into the surrounding medium, a local volume concentration can thus be estimated as $C_{L5}^{local\ volume} = C_{L5}^{surface}/h$. Even if h is assumed to be as large as 100 μm, the resulting local volume concentration initially exceeds both the MIC and MBC. $C_{L5}^{local\ volume}$ for h = 100 μm is 340 and 570 μg/mL, respectively, for the low and high-density microgel-modified surfaces. Over time, this concentration would decrease as L5 is released from the surface and diffuses into the surrounding medium. Clearly, however, the microgels act as reservoirs that maintain a high local concentration of antimicrobial agent despite the fact that the systemic concentration is low.

There are at least three possible mechanisms by which L5 can be released from the gels to inhibit bacterial colonization.

One is that the L5 slowly elutes from the gels over time consistent with many established drug-delivery strategies. However, as shown by Pavlukhina et al.,[69] L5 is slowly released from continuous thin films of poly(acrylic acid) hydrogels only when the pH is decreased to protonate the acid groups that electrostatically bind the L5. A second possible mechanism is that, because of their metabolic processes, colonizing bacteria will locally lower the pH. This mechanism would only trigger release from that surface area in close proximity to the colonizing bacteria. A third possible mechanism would be due to contact killing.[70] This is driven by gradients in chemical potential of the peptide when a bacterium gets sufficiently close to a loaded gel particle. Chemical potential differences can arise both because of the net negative charge of a bacterium cell wall at physiological pH[71,72] and because of the steep concentration difference between a loaded gel and a bacterial cell wall. In this case again, L5 would be released from the microgel locally due to the attraction between an individual bacterium and the peptide. The peptide would be released only when needed, thus preserving a high local L5 concentration over relatively long periods of time.

4. CONCLUSIONS

We have explored the synthesis, the physical properties, and self-assembly of PEG-based microgels with which to enhance the ability of a synthetic surface to resist bacterial colonization. We used suspension polymerization to synthesize pure PEG and PEG-*co*-acrylic acid microgels, both of which can be deposited onto poly(L-lysine)-primed silicon substrates. We were able to control the microgel surface density by the deposition time and the concentration of microgels in the parent colloidal suspension. We then used a polycationic peptide (L5) to show that the microgels can be loaded, again by self-assembly, and used as reservoirs for antimicrobial delivery. Because of the additional ionic bonding afforded by the acid groups, the loading of the acrylic-acid-containing microgels was much higher than that of pure PEG microgels. We assessed the ability of surfaces modified both by unloaded PEG-AA microgels and by L5-loaded PEG-AA microgels to resist the short-term colonization by *S. epidermidis*, a bacterium commonly implicated clinically in biomaterial-associated infection. Surfaces with both as-deposited and L5-loaded microgels inhibit bacterial colonization relative to unmodified control surfaces, and we can attribute this effect to the net surface repulsiveness an approaching bacterium experiences when the average spacing between microgels is about the same micrometer size of the bacterium itself. This effect is substantially amplified by the additional loading of L5 into microgels, an effect we attribute to the fact that, while the systemic concentration of L5 is relatively low, the concentration at the substrate surface exceeds both the minimum inhibitory and bactericidal concentrations.

Self-assembled microgels offer an innovative means with which to modify biomaterial surfaces. While able to achieve similar lateral modulations of surface cell-adhesiveness possible using lithographic patterning approaches, as a nonline-of-sight deposition process, microgel self-assembly can be applied to topographically complex surfaces over relatively large areas in a parallel fashion. However, in contrast to the various layer-by-layer self-assembly techniques to create thin films, microgel self-assembly can achieve significant surface modification with only one deposition step. In addition to their intrinsic antifouling properties, PEG-based microgels can also be used as reservoirs for localized drug delivery, the nature of which can be tuned by the extent and strength of hydrogen and ionic bonding present within individual microgels.

■ ASSOCIATED CONTENT

Supporting Information

(i) The pH-sensitive swelling behavior of bulk PEG-AA gels; (ii) the antimicrobial susceptibility of two strains of *S. epidermidis* to L5 and vancomycin; and (iii) the retention of FITC-L5 in PEG-AA microgels immersed in buffer. This material is available free of charge via the Internet at http://pubs.acs.org.

■ AUTHOR INFORMATION

Corresponding Author

*E-mail: mlibera@stevens.edu.

Notes

The authors declare no competing financial interest.

■ ACKNOWLEDGMENTS

The authors thank Prof. Jeff Kaplan of the New Jersey Dental School for providing the NJ9709 strain of *S. epidermidis* as well as Svetlana Pavlukhina and Prof. Svetlana Sukhishvili of Stevens for helpful conversations. This research project has been supported by the National Science Foundation through Grant #CBET-0708379 and used microscope resources partially funded by the National Science Foundation through NSF Grant DMR-0922522.

■ REFERENCES

(1) Chen, R.; Cole, N.; Willcox, M. D. P.; Park, J.; Rasul, R.; Carter, E.; Kumar, N. *Biofouling* **2009**, *25* (6), 517−524.
(2) Harris, L. G.; Mead, L.; Müller-Oberländer, E.; Richards, R. G. *J. Biomed. Mater. Res., Part A* **2006**, *78A* (1), 50−58.
(3) Lawson, M. C.; Bowman, C. N.; Anseth, K. S. *Clin. Orthop. Relat. Res.* **2007**, *461*, 96−105.
(4) Moskowitz, J. S.; Blaisse, M. R.; Samuel, R. E.; Hsu, H. P.; Harris, M. B.; Martin, S. D.; Lee, J. C.; Spector, M.; Hammond, P. T. *Biomaterials* **2010**, *31* (23), 6019−6030.
(5) Zhao, L.; Chu, P. K.; Zhang, Y.; Wu, Z. *J. Biomed. Mater. Res., Part B* **2009**, *91* (1), 470−480.
(6) Weaver, L.; Noyce, J. O.; Michels, H. T.; Keevil, C. W. *J. Appl. Microbiol.* **2010**, *109* (6), 2200−2205.
(7) Podsiadlo, P.; Paternel, S.; Rouillard, J.-M.; Zhang, Z.; Lee, J.; Lee, J.-W.; Gulari, E.; Kotov, N. A. *Langmuir* **2005**, *21* (25), 11915−11921.
(8) Monteiro, D. R.; Gorup, L. F.; Takamiya, A. S.; Ruvollo-Filho, A. C.; Camargo, E. R. d.; Barbosa, D. B. *Int. J. Antimicrob. Agents* **2009**, *34* (2), 103−110.
(9) Kostenko, V.; Lyczak, J.; Turner, K.; Martinuzzi, R. J. *Antimicrob. Agents Chemother.* **2010**, *54* (12), 5120−5131.
(10) Grunlan, J. C.; Choi, J. K.; Lin, A. *Biomacromolecules* **2005**, *6* (2), 1149−1153.
(11) Chen, W.; Liu, Y.; Courtney, H. S.; Bettenga, M.; Agrawal, C. M.; Bumgardner, J. D.; Ong, J. L. *Biomaterials* **2006**, *27* (32), 5512−5517.
(12) Cao, X. L.; Cheng, C.; Ma, Y. L.; Zhao, C. S. *J. Mater. Sci.: Mater. Med.* **2010**, *21* (10), 2861−2868.
(13) Hamm, S. C.; Shankaran, R.; Korampally, V.; Bok, S.; Praharaj, S.; Baker, G. A.; Robertson, J. D.; Lee, B. D.; Sengupta, S.; Gangopadhyay, K.; Gangopadhyay, S. *ACS Appl. Mater. Interfaces* **2012**, *4*, 178−184.
(14) Toppazzini, M.; Coslovi, A.; Boschelle, M.; Marsich, E.; Benincasa, M.; Gennaro, R.; Paoletti, S. *Carbohydr. Polym.* **2011**, *83* (2), 578−585.

(15) Murata, H.; Koepsel, R. R.; Matyjaszewski, K.; Russell, A. J. *Biomaterials* **2007**, *28* (32), 4870−4879.
(16) Li, B.; Jiang, B.; Boyce, B. M.; Lindsey, B. A. *Biomaterials* **2009**, *30* (13), 2552−2558.
(17) Khoo, X.; O'Toole, G. A.; Nair, S. A.; Snyder, B. D.; Kenan, D. J.; Grinstaff, M. W. *Biomaterials* **2010**, *31* (35), 9285−9292.
(18) Kazemzadeh-Narbat, M.; Kindrachuk, J.; Duan, K.; Jenssen, H.; Hancock, R. E.; Wang, R. *Biomaterials* **2010**, *31* (36), 9519−9526.
(19) Glinel, K.; Jonas, A. M.; Jouenne, T.; Leprince, J.; Galas, L.; Huck, W. T. *Bioconjugate Chem.* **2009**, *20* (1), 71−77.
(20) Dvoracek, C. M.; Sukhonosova, G.; Benedik, M. J.; Grunlan, J. C. *Langmuir* **2009**, *25* (17), 10322−10328.
(21) Patel, J. D.; Ebert, M.; Ward, R.; Anderson, J. M. *J. Biomed. Mater. Res., Part A* **2007**, *80* (3), 742−751.
(22) Chapman, R. G.; Ostuni, E.; Liang, M. N.; Meluleni, G.; Kim, E.; Yan, L.; Pier, G.; Warren, H. S.; Whitesides, G. M. *Langmuir* **2001**, *17* (4), 1225−1233.
(23) Desai, N. P.; Hossainy, S. F.; Hubbell, J. A. *Biomaterials* **1992**, *13* (7), 417−420.
(24) Khoo, X.; Hamilton, P.; O'Toole, G. A.; Snyder, B. D.; Kenan, D. J.; Grinstaff, M. W. *J. Am. Chem. Soc.* **2009**, *131* (31), 10992−10997.
(25) Kingshott, P.; Wei, J.; Bagge-Ravn, D.; Gadegaard, N.; Gram, L. *Langmuir* **2003**, *19* (17), 6912−6921.
(26) Koh, W.-G.; Revzin, A.; Simonian, A.; Reeves, T.; Pishko, M. *Biomed. Microdevices* **2003**, *5* (1), 11−19.
(27) Malmsten, M.; Emoto, K.; Van Alstine, J. M. *J. Colloid Interface Sci.* **1998**, *202* (2), 507−517.
(28) Ostuni, E.; Chapman, R. G.; Liang, M. N.; Meluleni, G.; Pier, G.; Ingber, D. E.; Whitesides, G. M. *Langmuir* **2001**, *17* (20), 6336−6343.
(29) Roosjen, A.; de Vries, J.; van der Mei, H. C.; Norde, W.; Busscher, H. J. *J. Biomed. Mater. Res., Part B* **2005**, *73* (2), 347−354.
(30) Wagner, V. E.; Koberstein, J. T.; Bryers, J. D. *Biomaterials* **2004**, *25* (12), 2247−2263.
(31) Elbert, D. L.; Hubbell, J. A. *Annu. Rev. Mater. Sci.* **1996**, *26* (1), 365−294.
(32) Gombotz, W. R.; Wang, G. H.; Horbett, T. A.; Hoffman, A. S. *J. Biomed. Mater. Res.* **1991**, *25* (12), 1547−1562.
(33) Gong, X.; Dai, L.; Griesser, H. J.; Mau, A. W. H. *J. Polym. Sci., Part B: Polym. Phys.* **2000**, *38* (17), 2323−2332.
(34) Hucknall, A.; Rangarajan, S.; Chilkoti, A. *Adv. Mater.* **2009**, *21* (23), 2441−2446.
(35) Israelachvili, J. *Proc. Natl. Acad. Sci. U. S. A.* **1997**, *94* (16), 8378−9.
(36) Prime, K. L.; Whitesides, G. M. *Science* **1991**, *252* (5010), 1164−1167.
(37) Prime, K. L.; Whitesides, G. M. *J. Am. Chem. Soc.* **1993**, *115* (23), 10714−10721.
(38) Revzin, A.; Rajagopalan, P.; Tilles, A. W.; Berthiaume, F.; Yarmush, M. L.; Toner, M. *Langmuir* **2004**, *20* (8), 2999−3005.
(39) Humphries, M.; Nemcek, J.; Cantwell, J. B.; Gerrard, J. J. *FEMS Microbiol. Lett.* **1987**, *45* (5), 297−304.
(40) Krsko, P.; Kaplan, J. B.; Libera, M. *Acta Biomater.* **2009**, *5* (2), 589−596.
(41) Roosjen, A.; van der Mei, H. C.; Busscher, H. J.; Norde, W. *Langmuir* **2004**, *20* (25), 10949−10955.
(42) Wang, Y.; Subbiahdoss, G.; Swartjes, J.; van der Mei, H. C.; Busscher, H. J.; Libera, M. *Adv. Funct. Mater.* **2011**, *21* (20), 3916−3923.
(43) Flory, P. J. *Principles of polymer chemistry*; Cornell University Press: Ithaca, 1953.
(44) Flory, P. J.; Rehner, J. J. *J. Chem. Phys.* **1943**, *11* (11), 521−526.
(45) Flory, P. J.; Rehner, J. J. *J. Chem. Phys.* **1943**, *11* (11), 512−520.
(46) Hiemenz, P. C.; Lodge, T. *Polymer chemistry*, 2nd ed.; CRC Press: Boca Raton, 2007; p xvii, 587 p.
(47) Merrill, E. W.; Dennison, K. A.; Sung, C. *Biomaterials* **1993**, *14* (15), 1117−1126.
(48) Krsko, P.; Sukhishvili, S.; Mansfield, M.; Clancy, R.; Libera, M. *Langmuir* **2003**, *19* (14), 5618−5625.
(49) Slaughter, B. V.; Khurshid, S. S.; Fisher, O. Z.; Khademhosseini, A.; Peppas, N. A. *Adv. Mater.* **2009**, *21* (32−33), 3307−3329.
(50) Mellott, M. B.; Searcy, K.; Pishko, M. V. *Biomaterials* **2001**, *22* (9), 929−941.
(51) Kofinas, P.; Athanassiou, V.; Merrill, E. W. *Biomaterials* **1996**, *17* (15), 1547−1550.
(52) Erol, M.; Du, H.; Sukhishvili, S. *Langmuir* **2006**, *22* (26), 11329−11336.
(53) Rasband, W. S. *ImageJ*; U. S. National Institutes of Health: Bethesda, Maryland, 1997−2009.
(54) Rosin, P. R., E. *J. Inst. Fuel* **1933**, *7*, 29−36.
(55) Tu, Z.; Volk, M.; Shah, K.; Clerkin, K.; Liang, J. F. *Peptides* **2009**, *30* (8), 1523−1528.
(56) CLSI. *Methods for dilution antimicrobial susceptibility tests for bacteriathat grow aerobically*, 8 ed.; CLSI document M07-A8. Clinical and Laboratory Standards Institute: Wayne, PA, 2009.
(57) Kaplan, J. B.; Ragunath, C.; Velliyagounder, K.; Fine, D. H.; Ramasubbu, N. *Antimicrob. Agents Chemother.* **2004**, *48* (7), 2633−2636.
(58) Sukhishvili, S. A.; Granick, S. *Macromolecules* **2001**, *35* (1), 301−310.
(59) Choi, J.; Rubner, M. F. *Macromolecules* **2004**, *38* (1), 116−124.
(60) Schmidt, M. *J. Phys.: Condens. Matter* **2002**, *14* (46), 12119−12127.
(61) Schmidt, S.; Hellweg, T.; von Klitzing, R. *Langmuir* **2008**, *24* (21), 12595−12602.
(62) Qiu, H.; Lee, W. Y.; Sukhishvili, S. A. *J. Am. Ceram. Soc.* **2006**, *89* (4), 1180−1187.
(63) South, A. B.; Whitmire, R. E.; Garcia, A. J.; Lyon, L. A. *ACS Appl. Mater. Interfaces* **2009**, *1* (12), 2747−2754.
(64) Chou, P. Y.; Fasman, G. D. *Annu. Rev. Biochem.* **1978**, *47*, 251−276.
(65) Harpaz, Y.; Gerstein, M.; Chothia, C. *Structure* **1994**, *2* (7), 641−649.
(66) Wei, Y.; Latour, R. A. *Langmuir* **2008**, *24* (13), 6721−6729.
(67) Lustig, S. R.; Peppas, N. A. *J. Appl. Polym. Sci.* **1988**, *36* (4), 735−747.
(68) Crank, J. *The mathematics of diffusion*, 2d ed.; Clarendon Press: Oxford, [Eng], 1975; p viii, 414 p.
(69) Pavlukhina, S.; Lu, Y.; Patimetha, A.; Libera, M.; Sukhishvili, S. *Biomacromolecules* **2010**, *11* (12), 3448−3456.
(70) Tiller, J. C.; Liao, C.-J.; Lewis, K.; Klibanov, A. M. *Proc. Natl. Acad. Sci. U. S. A.* **2001**, *98* (11), 5981−5985.
(71) Habash, M. B.; van der Mei, H. C.; Busscher, H. J.; Reid, G. *Colloids Surf., B* **2000**, *19* (1), 13−17.
(72) Wilson, W. W.; Wade, M. M.; Holman, S. C.; Champlin, F. R. *J. Microbiol. Methods* **2001**, *43* (3), 153−164.